Contact
Volume 6: 1–10

DOI: 10.1177/25152564231157706
journals.sagepub.com/home/ctc

An Expansion of the Endoplasmic Reticulum that Halts Autophagy is Permissive to Genome Instability

Eliana Lara-Barba[1], Alba Torán-Vilarrubias[1], and María Moriel-Carretero[2]

Abstract

The links between autophagy and genome stability, and whether they are important for lifespan and health, are not fully understood. We undertook a study to explore this notion at the molecular level using *Saccharomyces cerevisiae*. On the one hand, we triggered autophagy using rapamycin, to which we exposed mutants defective in preserving genome integrity, then assessed their viability, their ability to induce autophagy and the link between these two parameters. On the other hand, we searched for molecules derived from plant extracts known to have powerful benefits on human health to try to rescue the negative effects rapamycin had against some of these mutants. We uncover that autophagy execution is lethal for mutants unable to repair DNA double strand breaks, while the extract from *Silybum marianum* seeds induces an expansion of the endoplasmic reticulum (ER) that blocks autophagy and protects them. Our data uncover a connection between genome integrity and homeostasis of the ER whereby ER stress-like scenarios render cells tolerant to sub-optimal genome integrity conditions.

Keywords

endoplasmic reticulum, autophagy, genome instability, DNA DSBs, homologous recombination, *Silybum marianum*

Introduction

Dietary restriction, the minimal food intake allowing satisfaction of vital needs, extends healthy lifespan from yeast to humans (Fontana et al., 2010), as slowing down metabolic activity by reducing food intake is thought to delay the aging process (López-Otín et al., 2016). Its benefits are also linked to an improved maintenance of genome stability (Vermeij et al., 2016), having strong implications for therapy of both degenerative and cancer-related diseases (Mihaylova et al., 2014). Dietary restriction inhibits TOR, a master complex coordinating cell growth and metabolic homeostasis, leading to a sharp halt in growth (Loewith & Hall, 2011). Rapamycin, a lipophilic macrolide first obtained from *Streptomyces hygroscopicus*, used in organ transplantation, cancer and coronary artery disease, inhibits TOR thus mimics this specific effect of dietary restriction. TOR inhibition triggers autophagy, a degradative process by which dispensable or damaged cellular components are degraded (Klionsky et al., 2007).

With the initial idea of exploring how dietary restriction, in general, and autophagy, more specifically, intersects with genome stability, we exposed *S. cerevisiae* mutants defective in preserving genome integrity to rapamycin. We also searched for molecules derived from powerful plant extracts having benefits on human health that support these mutants' growth. We uncover a connection between genome integrity and the homeostasis of the endoplasmic reticulum (ER), a key organelle for correct protein folding; lipid synthesis and modification; and calcium storage (Schwarz & Blower, 2016). We find that ER stress-like scenarios render cells tolerant to sub-optimal genome integrity and that autophagy can be tailored to manipulate this link. We also introduce the power of milk thistle, *Silybum marianum*, in doing so.

[1]Institut de Génétique Humaine (IGH), Université de Montpellier-Centre National de la Recherche Scientifique, Montpellier, France
[2]Centre de Recherche en Biologie cellulaire de Montpellier (CRBM), Université de Montpellier-Centre National de la Recherche Scientifique, Montpellier, France

Received September 23, 2022. Revised January 27, 2023. Accepted January 27, 2023

Corresponding Author:
María Moriel-Carretero, Centre de Recherche en Biologie cellulaire de Montpellier (CRBM), Université de Montpellier-Centre National de la Recherche Scientifique, Montpellier cedex 5, France.
Email: maria.moriel@crbm.cnrs.fr

Results and Discussion

DNA Repair Mutants Display Altered Autophagy Profiles

We selected *S. cerevisiae* strains mutant in pathways that maintain genome stability and scored their growth in medium plus a rapamycin dose at which the wild-type (WT) strain can grow. These included mutants defective in DNA double strand breaks (DSBs) repair by homologous recombination (HR), nucleotide and base excision repair and in replication proficiency (Figure 1A). Mutants lacking genes necessary to perform early stages of HR were specifically rapamycin-sensitive (Figure 1A, red). We chose cells lacking the DNA break early binder Mre11, and cells lacking the DNA homology searcher Rad52, as paradigms for subsequent experiments.

Since rapamycin induces autophagy, we first monitored this process using a plasmid expressing GFP-Atg8. Atg8 accumulates in growing phagophores and promotes the membrane nucleation necessary to wrap and engulf cargoes in mature autophagosomes (Figure 1B). Using this tool (Klionsky et al., 2007), these structures can be seen by fluorescence microscopy as foci. Additionally, autophagy completion when autophagosomes fuse with the vacuole renders it fluorescent, since the GFP moiety better resists degradation (Figure 1B). This lysis can also be assessed by western blot (WB), because the released GFP runs faster in gel than undigested GFP-Atg8. WT, *mre11Δ* and *rad52Δ* cells of two different genetic backgrounds (namely W303 and BY4741) expressing GFP-Atg8 were either treated or not with rapamycin. WT cells displayed a low basal level of GFP-Atg8 foci and even lower vacuolar signals, while rapamycin treatment resulted in effective autophagy execution, as expected (Figure 1C and D, GFP signals). In both *mre11Δ* and *rad52Δ* cells, rapamycin addition triggered autophagy implementation with very similar profiles to that shown by the WT, and this irrespective of the genetic background (Figure 1C and D, GFP signals). Interestingly, however, both *mre11Δ* and *rad52Δ* displayed very high levels of GFP-Atg8 puncta but not vacuolar signals in basal conditions in the W303 background, as if basal Atg8-containing structures were accumulating (Figure 1C and D). In all cases, and since rapamycin kills these cells (Figure 1A), we conclude that the inability of *mre11Δ* and *rad52Δ* cells to grow in rapamycin does not stem from an inability to execute autophagy.

Silybum marianum Halts Autophagy Execution

To understand why rapamycin treatment is lethal in HR-deficient backgrounds, we searched for molecules reverting this phenotype. We used 13 ancestrally known plant extracts having beneficial effects on health (Swerdlow, 2000) on agar plates + rapamycin and tried to rescue the growth defect of *mre11Δ* (Figure S1). While roughly half of them had no major effect and the other half had a general antibiotic effect, two of them, namely extract from aerial parts of *Filipendula ulmaria,* and extract from *Silybum marianum* seeds, restored viability (Figure S1). We further studied *S. marianum*, as it is commonly used in the clinics to treat cirrhosis and liver poisoning. The ability of *S. marianum* to bypass rapamycin-imposed growth delay was further validated for *rad52Δ* and *mre11Δ* (Figure 2A). By studying WT cells' morphological parameters by flow cytometry, we found this suppression was not simply due to the extract preventing rapamycin from entering into the cells. Indeed, cells treated with rapamycin increase their size (Figure 2B, right panel, red points) because of vacuolar growth (Loewith & Hall, 2011), yet the extract did not simply revert cell size back to an untreated-like pattern (Figure 2B, black points), but counteracted it by a gain in granularity (Figure 2B, right panel, cyan points) even in the absence of rapamycin (Figure 2B, left panel, violet points). Thus, the extract activity is not merely due to the prevention of rapamycin entry into the cells.

We saw by WB that *S. marianum* reduced WT basal autophagy levels (Figure 2C), and antagonized the autophagy induced by rapamycin (Figure 2C), and this epistatically to the absence of Atg1, the kinase ensuring membrane supply to the growing phagophore (Klionsky et al., 2007) (Figure 2C). To understand whether the extract prevented autophagy initiation or completion, we monitored GFP-Atg8 foci, and observed that the extract alone did not lead to any major effect in the W303 WT strain (Figure 2D). Yet, plus rapamycin, the extract effect became very apparent, resulting in more cells with foci at the expense of a significant decrease in cells with vacuolar GFP-Atg8 signals, as compared to rapamycin-only treatment (Figure 2D). The same results were obtained in a different genetic background (BY4741) and when assessed in both *mre11Δ* and *rad52Δ* cells, both by WB (Figure 2E) and microscopy (Figure 2F). Thus, the extract inhibits the step(s) of autophagy measurable as vacuolar degradation.

These data suggested that the rapamycin lethality seen in the mutants could relate to a toxic impact of autophagy completion. To evaluate this possibility, we prevented autophagy execution by removing the protein Atg1 (Figure 2C), and observed that, when exposed to rapamycin, *atg1Δ mre11Δ* cells were more rapamycin-resistant than *mre11Δ* alone (Figure 2G). Thus, autophagy completion seems to be toxic for HR mutants.

The Presence of Atg8 Foci Matches an ER Expansion

At this point, we knew that: (1) rapamycin-induced autophagy is lethal for HR mutants; (2) GFP-Atg8 foci accumulation correlates with viability in these mutants when exposed to rapamycin; (3) *S. marianum* antagonizes rapamycin lethality; (4) *S. marianum* antagonizes rapamycin-induced

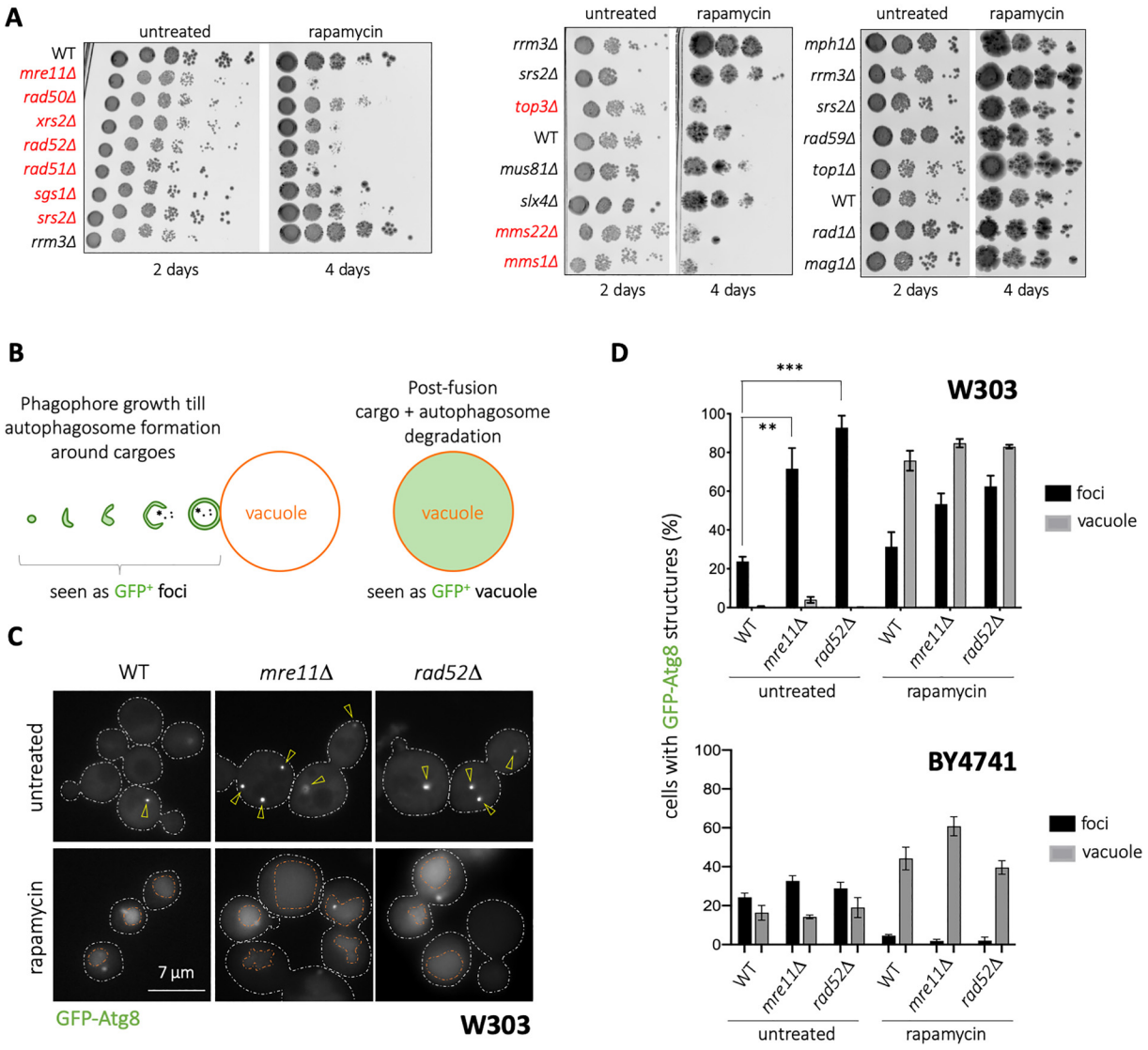

Figure 1. Mutants Deficient in HR are Sensitive to Rapamycin. A. 10-Fold serial dilutions of the indicated strains were spotted onto YPD plates + 5 ng mL^{-1} rapamycin then incubated at 30°C. Mutant cells lack proteins implicated in early DSB repair by HR (Mre11, Rad50, Xrs2 (the MRX complex), the homology search factors Rad52, Rad51, the Sgs1-Top3 complex, and the Mms1-Mms22 complex); late-acting in DSB repair and chromosome topological constraints resolution (Rad59, Slx4, Mus81, Srs2, Top1); nucleotide excision repair (Rad1); base excision repair (Mag1); and in replication fork progression (Rrm3, Mph1). B. Scheme illustrating how the GFP-Atg8 construct allows the detection of early phagophore nucleation and growth till mature autophagosome (seen as foci) then, cargo delivery and lysis within the vacuole (seen as vacuolar signals). C. Cells expressing GFP-Atg8 treated or not with 200 ng mL^{-1} rapamycin for 2 hours were seen under the fluorescence microscope. Dashed white lines define the cell perimeter, dashed orange lines define the vacuole perimeter, and yellow arrowheads point at GFP-Atg8 foci. D. Percentage of cells displaying the indicated structures (foci or vacuoles) for each strain and condition. Top: in a W303 genetic background. Bottom: in a BY4741 background. The bar height represents the mean of three independent experiments, and error bars the associated standard error of the mean. At least 200 cells were considered per experiment, cell type and condition. The asterisks indicate the statistical difference between the means after applying a one-way unpaired ANOVA test: $^{**}p < 0.01$; $^{***}p < 0.001$.

autophagy completion. To understand the events stabilizing GFP-Atg8 foci, we searched the bibliography for previous publications reporting these structures, and found similar patterns in cells treated with dithiothreitol (DTT) and tunicamycin (Bernales et al., 2006; Ghavidel et al., 2015). Both stressors of the ER, these agents provoke the accumulation of misfolded proteins, activating the unfolded protein response (UPR). Among other actions, the UPR elicits ER expansion (Ron & Walter, 2007). We confirmed DTT causes Atg8 foci accumulation (Figure 3A). The similarity between GFP-Atg8 foci in HR mutants (Figure 1C) and in DTT-treated WT (Figure 3A) prompted us to check if

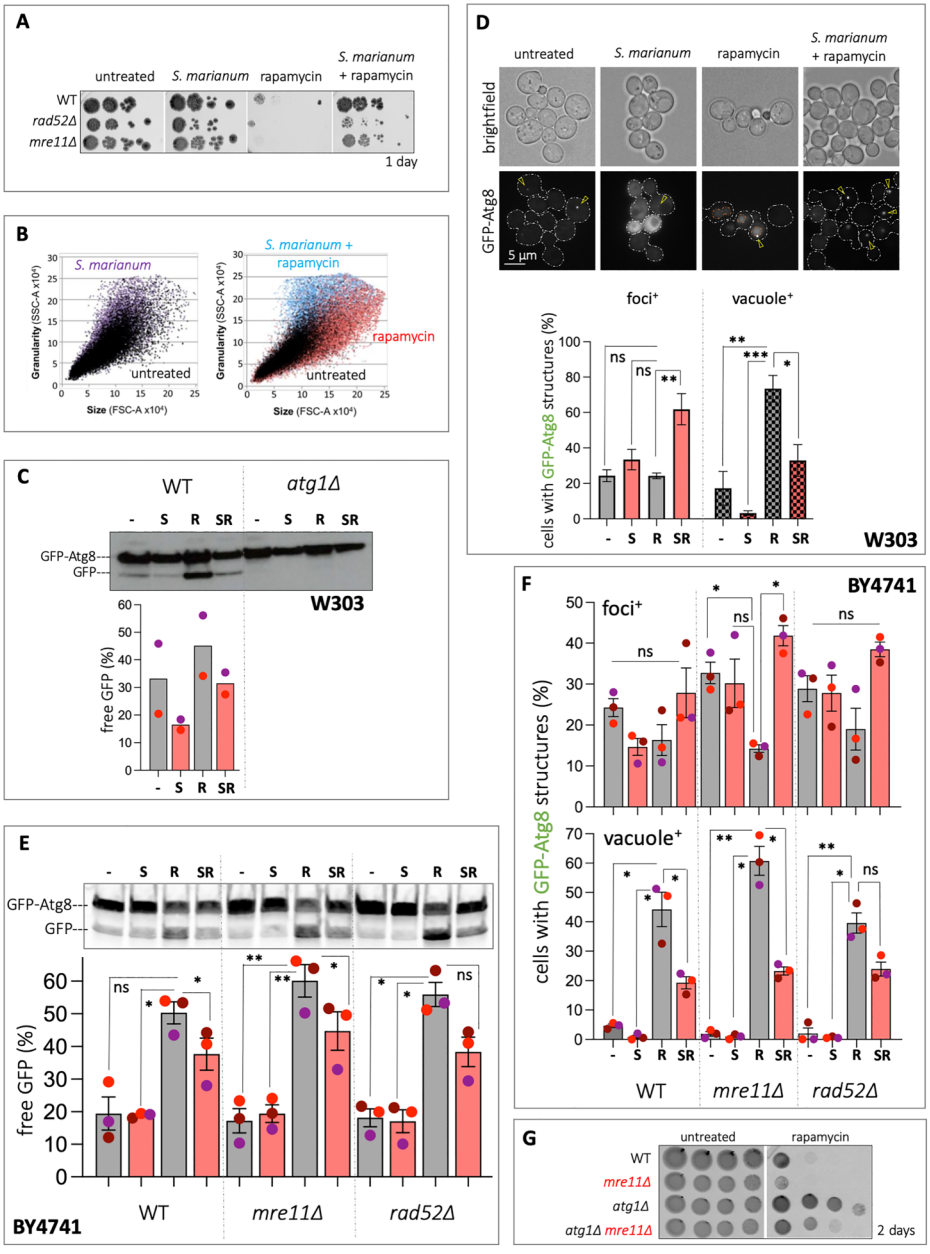

Figure 2. The Extract from *Silybum marianum* Seeds Antagonizes Rapamycin-Induced Autophagy. A. 10-Fold serial dilutions of the indicated cultures were spotted onto YPD plates + treatments and incubated at 30°C. "Untreated" plates contain 1% ethanol, the extract solvent. B. Cytometry was used to measure size (FSC-A) and granularity (SSC-A) of the WT strain subjected or not to 5 ng mL^{-1} and/or 5% *S. marianum* for 2 h. Each dot represents one cell. At least 10,000 cells are represented per treatment using the indicated color code. C. WB of WT W303 protein extracts detecting GFP-Atg8 and free GFP, indicative of vacuolar degradation. Treatments were 2-hour-long. Individual dots relate to independent experiments. The bar height indicates the mean value of free GFP signals in a lane with respect to all GFP signals. *atg1Δ* cells were used to eliminate the ability to accomplish autophagy. D. W303 cells treated as in (C) seen under the fluorescence microscope. Top: dashed white lines define the cell perimeter, dashed orange lines the vacuole perimeter, and yellow arrowheads GFP-Atg8 foci. Bottom: percentage of cells displaying foci or vacuoles for each strain and condition. The bar height represents the mean of three independent experiments, and error bars the associated standard error of the mean. At least 200 cells were considered per experiment, cell type and condition. An unpaired (3 or 4 independent experiments were considered) one-way ANOVA test comparing to the +rapamycin condition was applied to each category (foci / vacuole). $^{**}p < 0.01$; $^{*}p < 0.05$; ns, non-significant. E. Experimental details as in (C) but for WT and mutants of BY4741 background. Each colored dot relates to one independent experiment. A paired one-way ANOVA test comparing to the +rapamycin condition was applied to each genetic background. $^{**}p < 0.01$; $^{*}p < 0.05$; ns, non-significant. F. Experimental details as in (D) but for WT and mutants of BY4741 background. Each colored dot relates to one independent experiment. A paired one-way ANOVA test comparing to the +rapamycin condition was applied to each genetic background. $^{**}p < 0.01$; $^{*}p < 0.05$; ns, non-significant. G. 10-fold serial dilutions of the indicated cultures were spotted onto YPD plates ±5 ng mL^{-1} rapamycin and incubated at 30°C.

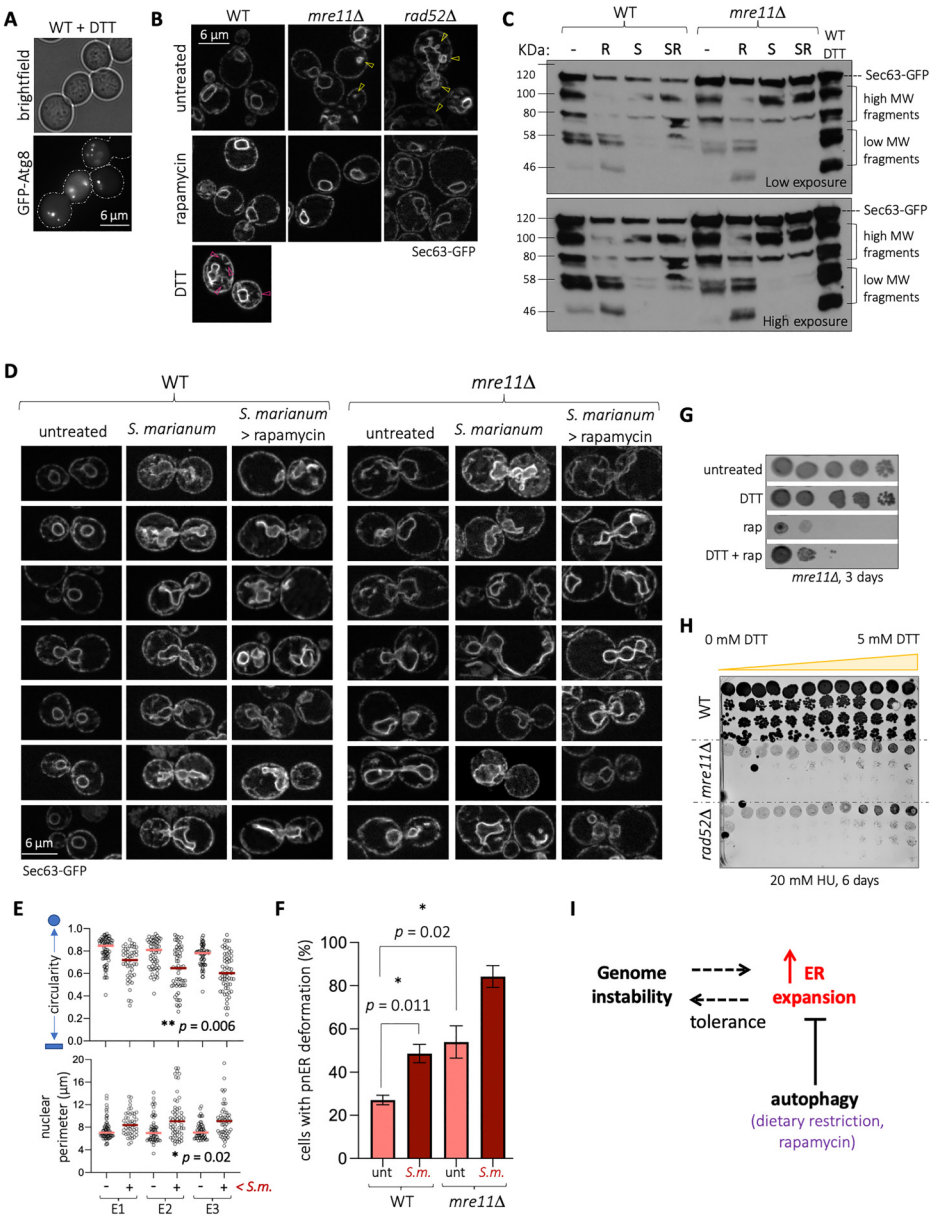

Figure 3. Autophagy is Counteracted by an ER Expansion. A. Example of WT cells treated with 8 mM DTT 2 hours to illustrate GFP-Atg8 foci accumulation. B. WT and mutant cells expressing Sec63-GFP were imaged after being treated (or not) with 200 ng mL^{-1} rapamycin (ER alterations are indicated by yellow arrowheads). Also, WT treated with 8 mM DTT for 2 hours is shown to illustrate the expansion of the cytoplasmic ER network (pink arrowheads). C. WB detecting Sec63-GFP and its derived fragments, indicative of vacuolar degradation. Treatments (200 ng mL^{-1} rapamycin; 5% *S. marianum*; 8 mM DTT) were applied for 2 hours. D. Details as in (B) but pre-treating or not WT and *mre11Δ* cells for 2 hours with 5% *S. marianum*. E. The perimeter of nuclei in WT cells treated or not with 5% *S. marianum* 2 hours was defined using ImageJ and two parameters, circularity (top) and perimeter length (bottom) were assessed in three independent experiments (E1, E2, E3), which are plotted. Each individual dot relates to one nucleus and the colored horizontal bar indicates the mean value. Asterisks indicate the statistical difference between the three means after applying an unpaired *t*-test. F. The experimental set-up was applied as in (D) to measure the percentage of WT and *mre11Δ* cells in the population displaying deformed nuclei. Asterisks indicate the statistical difference between the means after applying an unpaired one-way ANOVA test. G. 10-Fold serial dilutions of an *mre11Δ* culture were spotted onto YPD plates + treatments and incubated at 30°C. H. Four 10-fold serial dilutions of each strain were spotted all along a YPD plate homogeneously containing HU and a gradient of DTT and incubated at 30°C. I. Model recapitulating the main findings of this work. Cells experiencing genome instability, mostly inability to repair DSBs, display an expanded ER, a phenomenon that increases their tolerance to such instability. However, forcing autophagy completion with rapamycin ends up ER expansion, causing lethality. ER expansion and autophagy thus appear mutually exclusive, presumably by a competition for membrane availability or Atg8ylation. In this context, supporting ER expansion, as with *S. marianum* (or DTT), counteracts autophagy thus promotes viability of genome instability-bearing cells.

mre11Δ and *rad52Δ*, which in the W303 background displayed frequent GFP-Atg8 foci basally (Figure 1C and D), suffered from ER stress-like changes. To this end, we monitored Sec63-GFP, an integral ER membrane protein that allows following ER dynamics (expansion, fragmentation) by microscopy, and ER destruction (e.g., +rapamycin) by WB, when Sec63-GFP becomes cleaved into discrete fragments (Prinz et al., 2000; Schuck et al., 2014). WT cells displayed a normal ER distribution while mutant cells displayed a more complex ER, indicative of expansion, ER-derived vesicles and ER fragments reminiscent of whorls (Schuck et al., 2014) (Figure 3B, yellow arrowheads). Of note, addition of rapamycin, which instructed ER degradation by autophagy (Figure 3C), substantially normalized the aspect of the ER network (Figure 3B). As the ER is a major donor for autophagic membranes (Graef et al., 2013), data suggest that the GFP-Atg8 foci accumulation in *mre11*Δ and *rad52Δ* could stem from a shortage in membranes as a consequence of a developed ER network. It also suggests that maintaining an ER stress-like status could be beneficial for these mutants.

S. marianum Supports an ER Membrane Expansion That Helps Tolerate Genome Instability

Last, given that *S. marianum* extract rescued *mre11Δ* and *rad52Δ* lethality in rapamycin, that it antagonized autophagy by stabilizing GFP-Atg8 structures, and that mutants and GFP-Atg8 puncta share a link with ER expansions, we asked whether the extract action also relates to ER transitions. We observed that pre-treating WT or *mre11Δ* cells with the extract strongly protected their ER from rapamycin-induced degradation (Figure 3C). Also, extract-treated WT and *mre11Δ* cells were found to display an ER morphology reminiscent of an ER stress, yet not identical to a canonical unfolded protein one. In fact, DTT leads to an overgrowth of, mostly, the cytoplasmic ER subdomain (Figure 3B, pink arrowheads), while the extract led to a very marked expansion mostly at the perinuclear ER subdomain (Figure 3D). This expansion was robustly quantified both as a loss of nuclear circularity (Figure 3E, top), an increased nuclear periphery (Figure 3E, bottom), as well as more cells in the population displaying these phenotypes (Figure 3F). Importantly, and in agreement with the fact that the extract protected ER from rapamycin-induced degradation (Figure 3C), *S. marianum* prevented rapamycin from simplifying the ER network in both WT and *mre11Δ* cells (Figure 3D), in contrast to rapamycin alone (Figure 3B). Last, we asked whether the ER expansion helps tolerate genome instability. To assess this, we first exposed mutant cells to rapamycin and combined it or not with DTT, finding that DTT counteracts the lethality seen in rapamycin (Figure 3G). Second, we exposed all cells to a constant dose of the genotoxin hydroxyurea to which the WT is resistant while the mutants are sensitive, and onto a gradient of DTT. We found that increasing doses of DTT progressively led, slightly but reproducibly, to growth of the mutants (Figure 3H). Thus, we propose that the extract antagonizes autophagy by supporting an overgrown ER, and that ER expansions provide tolerance against genome instability.

A Model for ER Expansion as a Means to Tolerate Genome Instability

In this work, we show that GFP-Atg8 accumulation during genome instability correlates with cell survival, and *vice versa.* This compromises autophagy due to ER expansion, in agreement with the notion that autophagy and ER expansion counterbalance each other (Bernales et al., 2006). As such, HR-deficient cells become specifically sensitive upon autophagy implementation, presumably due to membrane shortage. Why are these mutants dependent on ER expansion, which also occurs in response to DSBs in human and mouse glial cells (Chatterjee et al., 2018; Zheng et al., 2018), to survive? In cells arrested in G_2, autophagy implementation allows the transition through mitosis (Matsui et al., 2013). Since cells with DSBs suffer a checkpoint-mediated arrest in G_2 preventing division prior to problem resolution (O'Connell et al., 2000), perhaps inhibiting autophagy ensures optimal G_2 retention. Alternatively, the autophagy halt could be a by-product of the need of an expanded ER and, even more excitingly, the GFP-Atg8 foci could stem from a competition for ATG8ylation between autophagy and membrane remodeling. Indeed, membrane lipids emerge as requesting their conjugation to Atg8 moieties as a general response to membrane stress and reshaping, a process that would compete with autophagy for Atg8 conjugates (Kumar et al., 2021).

But, what underlies this need for membrane? We observe that, in both *mre11Δ* and in *rad52Δ*, and in WT cells exposed to *S. marianum*, the main ER subdomain expanding is the perinuclear one, a.k.a. the nuclear envelope. It is known that the repair of DNA DSBs requests relocation to and contact with the nuclear envelope (Nagai et al., 2008; Oza et al., 2009; Ryu et al., 2015; Therizols et al., 2006), and that defined nuclear envelope regions, namely around the nucleolus, suffer lipid-driven expansions upon DSB-making treatments, among other elicitors (Garcia et al., 2022; Witkin et al., 2012). Of note, boosting the basally oxidative environment of the ER lumen elicits perinuclear ER subdomain deformations reminiscent to lipid stress (Torán-Vilarrubias & Moriel-Carretero, 2021). Moreover, the same *mrx* mutants used in this study display ER-born lipid alterations (Kanagavijayan et al., 2015), and *S. marianum* regulates lipid metabolism (Barbagallo et al., 2016). Last, *Filipendula ulmaria*, the other extract rescuing HR mutants lethality in rapamycin (Figure S1), strongly protects lipids from oxidation

(Katanić et al., 2015). It would be important to disclose the connection between an oxidative ER environment, lipid alterations, nuclear envelope expansion and DNA breaks tolerance (Figure 3I).

An important question is how, molecularly, ER expansion supports tolerance to genome instability. Defects in vesicular transport operating between the ER and the Golgi compromise the tolerance to both endogenous (Alvaro et al., 2007) and exogenous DSBs (Krol et al., 2015; Reid et al., 2011). The activation of the UPR is required for chromosome maintenance (Henry et al., 2010), although ER expansion can alleviate ER stress independently of the UPR (Schuck et al., 2009), enhancing replicative capacity (Ghavidel et al., 2015). This points to UPR-independent means by which the ER could buffer genome instability. In mammalian cells, loss of ER homeostasis also triggers responses beyond the UPR through regulated IRE1α-dependent mRNA decay (RIDD). This RNA processing targets thus attenuates mRNAs implicated in the DNA damage response (DDR) (Dufey et al., 2020), creating the means for adaptation, through which cells with persistent DNA breaks can resume normal activities without repairing. Further, reorganization of the ER sterol composition dictates the intensity of the DDR in response to DSBs through the selective titration of its kinase ATM (Ovejero et al., 2022).

Another relevant concern is the molecular pathway(s) elicited by the plant extract, which end up with the establishment of ER stress-like structures, thus tolerance to genome instability. Given the numerous molecules present in the extract, several different process(es) could underlie this phenomenon. In particular, *S. marianum* active molecules have been reported to both stimulate (Bai et al., 2018; Jiang et al., 2015; Kauntz et al., 2011; Li et al., 2022; Rezabakhsh et al., 2018) and antagonize (Song et al., 2017; Wang et al., 2013) autophagy in different cell systems, highlighting a complexity that should not be forgotten. In our set-up, though, autophagy induction by rapamycin imposes an intransigent context to cells deficient in DSB repair, in line with pioneer reports (Ferrari et al., 2017; Klermund et al., 2014; Vermeij et al., 2016). This could limit progression of certain pathological conditions, such as cancer. On the contrary, *S. marianum* appears as a strong candidate to treat degenerative diseases where exacerbated autophagy forces premature cell death and tissue loss. For example, the inactivation of Rint1, a factor interacting with the MRX component Rad50 (Figure 1A), implicated in radiation response in G_2 (Xiao et al., 2001), triggers in mouse neurons the same phenotypes we describe here for *S. cerevisiae*: genome instability, ER stress and autophagy halt. Further, the severe developmental defects and neurodegeneration associated Rint1 lack worsen upon rapamycin treatment (Grigaravicius et al., 2016). It will be of therapeutic interest to deepen in how the triangle genome stability / ER expansion / autophagy can be modulated (Figure 3I).

Materials and Methods

Strains, Plasmids, Culture, and Treatments

Strains possess either a W303 or a BY4741 background, comparisons were made with an isogenic WT. The pGFP-Atg8::*URA3* and pSec63-GFP::*URA3* plasmids were kind gifts of Chin-Chuan Chen (Chang Gung University, Taiwan) and Sebastian Schuck (University of Heidelberg, Germany), respectively. Most experiments were performed in either YPD (yeast extract, peptone with dextrose 2%) and YNB (yeast nitrogen base w/o amino acids, $(NH_4)_2SO_4$, tyrosine, dextrose 2% and basic supplement of amino acids). Treatments were as follows: 1% plant extract if in plates, 5% if in liquid medium; 5 ng mL^{-1} rapamycin if in plates, 200 ng mL^{-1} rapamycin if in liquid medium; 8 mM DTT in liquid cultures, gradient up to 5 mM DTT in plates; 20 mM hydroxyurea in plates. Plant extracts were bought prepared in ethanol from Avena Botanicals, Maine, USA. Other references are DTT (D9779, Sigma-Aldrich), rapamycin (HY-10219; Cliniscience), hydroxyurea (H8627; Sigma-Aldrich).

Sensitivity Assays on Plates

One tenth serially diluted cultures were spotted onto YPD plates containing ± 5 ng mL^{-1} rapamycin. For gradient assays (Figure S1), squared YPD plates homogeneously containing 5 ng mL^{-1} rapamycin were poured so that one side of the plate possessed virtually 0% extract, and the other side 1%, thus creating an extract gradient in between both (scheme in Figure S1, bottom). Cells were grown at 30°C and pictures taken every day.

Flow Cytometry Analyses

To acquire forward- and side-scattered light values (FSC-A and SSC-A, respectively) by flow cytometry, 430 µL of exponential culture cells were fixed with 1 mL of 100% ethanol, centrifuged for 1 minute at 16,000 *g* and resuspended in 500 µL 50 mM Na–citrate buffer containing 5 µL of RNase A (10 mg/mL, Euromedex, RB0474) for 2 h at 50°C. 6 µL of 20 mg/mL Proteinase K (Euromedex, EU0090-C) were added for 1 h at 50°C. Aggregates were dissociated by brief sonication. 20 µL of this cell suspension were incubated with 200 µL of 50 mM Na–citrate buffer containing 4 µg/mL propidium iodide (FisherScientific). Data were acquired on a MACSQuant Analyser X (Miltenyi Biotec) and analyzed with FlowJo software.

GFP-Atg8 and Sec63-GFP Fluorescence Microscopy Assays and Image Analysis

Cells from exponentially growing cultures were mounted on a coverslip for immediate imaging of the relevant signals,

detected using the adequate wavelength with a Zeiss CCD AxioCam MRm monochrome camera from a Zeiss AxioImager Z1 microscope with ApoTome technology using a 40× Plan Apochromat 1.3-NA oil objective lens and Zen software. Image visualization and analysis were performed with ImageJ v2.0.0-rc-69/1.52i. For defining nuclear peripheries to establish their circularity and perimeter length, a supervised threshold was chosen using ImageJ, objects created out of it, then these parameters automatically calculated out of those objects.

Western Blotting

Frozen pellets derived from 10 mL of exponentially growing cells were resuspended in 200 µL of pre-warmed (70°C) complete cracking buffer (8 M urea, 5%, w/v SDS, 40 mM Tris–HCl [pH 6.8], 0.1 mM EDTA, 0.4 mg mL^{-1} bromophenol blue, 150 mM β-mercaptoethanol, protease inhibitor cocktail, 2 mM PMSF), an equal volume of glass beads added to the tubes, and cells were lysed at 70°C by agitation for 20 min. Cell lysates were collected by centrifugation at 16,000 *g* for 15 minutes. To separate GFP from GFP-Atg8, extracts were separated in 4–20% acrylamide gel (Bio-Rad) and migrated 45 minutes at 100 V in MES buffer. To separate Sec63-GFP and derived fragments, proteins were separated in 7.5% acrylamide gels (Bio-Rad) and migrated 70 min at 100 V in Tris–glycine buffer. A nitrocellulose membrane was blocked in 10% milk, immunoblotting accomplished using an anti-GFP antibody (ab290, 1/2,000; Abcam) and an anti-rabbit HRP secondary antibody (A9044-2ML, 1/3,000; Sigma-Aldrich). To quantify free GFP signals, the total GFP signals in a lane were counted using ImageJ, and the percentage of free *versus* total signals was calculated.

Plots and Statistical Analyses

Graphical representations and statistical analyses were made with GraphPad Prism to both plot graphs and statistically analyze the data. Independent experiments refer in all cases to biological replicates. For data representation, we used the standard error of the mean, since all the considered measurements concerned a mean (the percentage of cells in the population bearing a given GFP-Atg8 signal), and the goal of our error bars was to describe the uncertainty of the true population mean being represented by the sample mean. In that line, we performed one-way ANOVA analyses to assess whether the means were statistically significantly different if more than one comparison was to be done, while *t*-tests (paired or unpaired, depending on the nature of the samples) were applied to compare two samples.

Acknowledgments

The authors acknowledge the imaging facility MRI, a member of the national infrastructure France-BioImaging, supported by the French National Research Agency (ANR-10-INBS-04, Investissements d'avenir), and the Fondation L'Oréal. They also thank the joint IGMM-CRBM "yeast media and technologies service" for providing them with ready-to-use media. They thank Philippe Pasero for hosting the execution of part of these experiments and for his unconditional support to the research in their laboratory. They are grateful to Sebastian Schuck for the gift of the pSec63p-GFP plasmid and to Dr. Chin-Chuan Chen and Pr. Wei-Pang Huang, Taiwan, for the present of pGFP-Atg8 and the *atg1Δ* strain.

Author Note

Currently, the author Eliana Lara-Barba is affiliated in Laboratorio de Inmunología Celular y Molecular, Centro de Investigación e Innovación Biomédica (CIIB), Facultad de Medicina, Universidad de Los Andes, Santiago, Chile.

Authors' Contributions

E.L.-B.: data curation, validation, investigation, visualization, methodology, and writing—original draft, review, and editing. A.T.-V.: data curation, validation, investigation, and writing—review, and editing. M.M.-C.: conceptualization, data curation, supervision, funding acquisition, validation, investigation, visualization, methodology, project administration, and writing—original draft, review, and editing.

Data Availability Statement

All the information relevant to the study is included within this manuscript. Additional requests will be satisfied by the corresponding author.

Declaration of Conflicting Interests

The author(s) declared no potential conflicts of interest with respect to the research, authorship, and/or publication of this article.

Funding

The author(s) disclosed receipt of the following financial support for the research, authorship, and/or publication of this article: This work was supported by FWIS program by Fondation L'Oréal-UNESCO; the ATIP-Avenir program; La Ligue contre le Cancer et l'Institut National du Cancer (PLBIO19-098 INCA_13832), France; and the Agence Nationale de la Recherche (ANR-21-CE12-0004-01), France.

ORCID iD


María Moriel-Carretero https://orcid.org/0000-0002-6770-3486

Supplemental Material

Supplemental material for this article is available online.

References

Alvaro, D., Lisby, M., & Rothstein, R. (2007). Genome-wide analysis of Rad52 foci reveals diverse mechanisms impacting recombination. *PLoS Genetics*, *3*, 2439–2449. https://doi.org/10.1371/journal.pgen.0030228

Bai, Z.-L., Tay, V., Guo, S.-Z., Ren, J., & Shu, M.-G. (2018). Silibinin induced human glioblastoma cell apoptosis concomitant with autophagy through simultaneous inhibition of mTOR

and YAP. *BioMed Research International*, *2018*, 1–10. https://doi.org/10.1155/2018/6165192

Barbagallo, I., Vanella, L., Cambria, M. T., Tibullo, D., Godos, J., Guarnaccia, L., Zappalà, A., Galvano, F., & Li Volti, G. (2016). Silibinin regulates lipid metabolism and differentiation in functional human adipocytes. *Frontiers in Pharmacology*, *6*, 1–10. https://doi.org/10.3389/fphar.2015.00309

Bernales, S., McDonald, K. L., & Walter, P. (2006). Autophagy counterbalances endoplasmic reticulum expansion during the unfolded protein response. *PLoS Biology*, *4*, 2311–2324. https://doi.org/10.1371/journal.pbio.0040423

Chatterjee, J., Nairy, R. K., Langhnoja, J., Tripathi, A., Patil, R. K., Pillai, P. P., & Mustak, M. S. (2018). ER Stress and genomic instability induced by gamma radiation in mice primary cultured glial cells. *Metabolic Brain Disease*, *33*, 855–868. https://doi.org/10.1007/s11011-018-0183-9

Dufey, E., Bravo-San Pedro, J. M., Eggers, C., González-Quiroz, M., Urra, H., Sagredo, A. I., Sepulveda, D., Pihán, P., Carreras-Sureda, A., Hazari, Y., Sagredo, E. A., Gutierrez, D., Valls, C., Papaioannou, A., Acosta-Alvear, D., Campos, G., Domingos, P. M., Pedeux, R., Chevet, E., & … Hetz, C. (2020). Genotoxic stress triggers the activation of IRE1α-dependent RNA decay to modulate the DNA damage response. *Nature Communications*, *11*, 1–13. https://doi.org/10.1038/s41467-020-15694-y

Ferrari, E., Bruhn, C., Peretti, M., Cassani, C., Carotenuto, W. V., Elgendy, M., Shubassi, G., Lucca, C., Bermejo, R., Varasi, M., Minucci, S., Longhese, M. P., & Foiani, M. (2017). PP2A controls genome integrity by integrating nutrient-sensing and metabolic pathways with the DNA damage response. *Molecular Cell*, *67*, 266–281. https://doi.org/10.1016/j.molcel.2017.05.027

Fontana, L., Partridge, L., & Longo, V. D. (2010). Extending healthy life span—From yeast to humans. *Science (New York, N.Y.)*, *328*, 321–326. https://doi.org/10.1126/science.1172539

Garcia, M., Kumanski, S., Elías-Villalobos, A., Cazevieille, C., Soulet, C., & Moriel-Carretero, M. (2022). Nuclear ingression of cytoplasmic bodies accompanies a boost in autophagy. *Life Science Alliance*, *5*, e202101160. https://doi.org/10.26508/lsa.202101160

Ghavidel, A., Baxi, K., Ignatchenko, V., Prusinkiewicz, M., Arnason, T. G., Kislinger, T., Carvalho, C. E., & Harkness, T. A. A. (2015). A genome scale screen for mutants with delayed exit from mitosis: Ire1-independent induction of autophagy integrates ER homeostasis into mitotic lifespan. *PLoS Genetics*, *11*, https://doi.org/10.1371/journal.pgen.1005429

Graef, M., Friedman, J. R., Graham, C., Babu, M., & Nunnari, J. (2013). ER exit sites are physical and functional core autophagosome biogenesis components. *Molecular Biology of the Cell*, *24*, 2918–2931. https://doi.org/10.1091/mbc.E13-07-0381

Grigaravicius, P., Kaminska, E., Hubner, C. A., McKinnon, P. J., Von Deimling, A., & Frappart, P. O. (2016). Rint1 inactivation triggers genomic instability, ER stress and autophagy inhibition in the brain. *Cell Death & Differentiation*, *23*, 454–468. https://doi.org/10.1038/cdd.2015.113

Henry, K. A., Blank, H. M., Hoose, S. A., & Polymenis, M. (2010). The unfolded protein response is not necessary for the G1/S transition, but it is required for chromosome maintenance in *Saccharomyces cerevisiae*. *PLoS One*, *5*, 1–10. https://doi.org/10.1371/journal.pone.0012732

Jiang, K., Wang, W., Jin, X., Wang, Z., Ji, Z., & Meng, G. (2015). Silibinin, a natural flavonoid, induces autophagy via ROS-dependent mitochondrial dysfunction and loss of ATP involving BNIP3 in human MCF7 breast cancer cells. *Oncology Reports*, *33*, 2711–2718. https://doi.org/10.3892/or.2015.3915

Kanagavijayan, D., Rajasekharan, R., & Srinivasan, M. (2015). Yeast MRX deletions have short chronological life span and more triacylglycerols. *FEMS Yeast Research*, *16*, 1–14. https://doi.org/10.1093/femsyr/fov109

Katanić, J., Boroja, T., Stanković, N., Mihailović, V., Mladenović, M., Kreft, S., & Vrvić, M. M. (2015). Bioactivity, stability and phenolic characterization of *Filipendula ulmaria* (L.) Maxim. *Food & Function*, *6*, 1164–1175. https://doi.org/10.1039/c4fo01208a

Kauntz, H., Bousserouel, S., Gossé, F., & Raul, F. (2011). Silibinin triggers apoptotic signaling pathways and autophagic survival response in human colon adenocarcinoma cells and their derived metastatic cells. *Apoptosis*, *16*, 1042–1053. https://doi.org/10.1007/s10495-011-0631-z

Klermund, J., Bender, K., & Luke, B. (2014). High nutrient levels and TORC1 activity reduce cell viability following prolonged telomere dysfunction and cell cycle arrest. *Cell Reports*, *9*, 324–335. https://doi.org/10.1016/j.celrep.2014.08.053

Klionsky, D. J., Cuervo, A. M., & Seglen, P. O. (2007). Methods for monitoring autophagy from yeast to human. *Autophagy*, *3*, 181–206. https://doi.org/10.4161/auto.3678

Krol, K., Brozda, I., Skoneczny, M., Bretne, M., & Skoneczna, A. (2015). A genomic screen revealing the importance of vesicular trafficking pathways in genome maintenance and protection against genotoxic stress in diploid *Saccharomyces cerevisiae* cells. *PLoS One*, *10*, 1–32. https://doi.org/10.1371/journal.pone.0120702

Kumar, S., Jia, J., & Deretic, V. (2021). Atg8ylation as a general membrane stress and remodeling response. *Cell Stress*, *5*, 128–142. https://doi.org/10.15698/cst2021.09.255

Li, W., Qu, X., Kang, X., Zhang, H., Zhang, X., Hu, H., Yao, L., Zhang, L., Zheng, J., Zheng, Y., Zhang, J., & Xu, Y. (2022). Silibinin eliminates mitochondrial ROS and restores autophagy through IL6ST/JAK2/STAT3 signaling pathway to protect cardiomyocytes from doxorubicin-induced injury. *European Journal of Pharmacology*, *929*, 175153. https://doi.org/10.1016/j.ejphar.2022.175153

Loewith, R., & Hall, M. N. (2011). Target of rapamycin (TOR) in nutrient signaling and growth control. *Genetics*, *189*, 1177–1201. https://doi.org/10.1534/genetics.111.133363

López-Otín, C., Galluzzi, L., Freije, J. M. P., Madeo, F., & Kroemer, G. (2016). Metabolic control of longevity. *Cell*, *166*, 802–821. https://doi.org/10.1016/j.cell.2016.07.031

Matsui, A., Kamada, Y., & Matsuura, A. (2013). The role of autophagy in genome stability through suppression of abnormal mitosis under starvation. *PLoS Genetics*, *9*, e1003245. https://doi.org/10.1371/journal.pgen.1003245

Mihaylova, M. M., Sabatini, D. M., & Yilmaz, Ö.H. (2014). Dietary and metabolic control of stem cell function in physiology and cancer. *Cell Stem Cell*, *14*, 292–305. https://doi.org/10.1016/j.stem.2014.02.008

Nagai, S., Dubrana, K., Tsai-Pflugfelder, M., Davidson, M. B., Roberts, T. M., Brown, G. W., Varela, E., Hediger, F., Gasser, S. M., & Krogan, N. J. (2008). Functional targeting of DNA

damage to a nuclear pore-associated SUMO-dependent ubiquitn ligase. *Science (New York, N.Y.)*, *322*, 597–602. https://doi.org/10.1126/science.1162790

O'Connell, M. J., Walworth, N. C., & Carr, A. M. (2000). The G2-phase DNA-damage checkpoint. *Trends in Cell Biology*, *10*, 296–303. https://doi.org/10.1016/S0962-8924(00)01773-6

Ovejero, S., Kumanski, S., Soulet, C., Azarli, J., Pardo, B., Santt, O., Constantinou, A., Pasero, P., & Moriel-Carretero, M. (2022). A Sterol-PI(4)P exchanger controls the Tel1/ATM axis of the DNA damage response. *bioRxiv*. https://doi.org/10.1101/2022.07.13.499867

Oza, P., Jaspersen, S. L., Miele, A., Dekker, J., & Peterson, C. L. (2009). Mechanisms that regulate localization of a DNA double-strand break to the nuclear periphery. *Genes & Development*, *23*, 912–927. https://doi.org/10.1101/gad.1782209

Prinz, W. A., Grzyb, L., Veenhuis, M., Kahana, J. A., Silver, P. A., & Rapoport, T. A. (2000). Mutants affecting the structure of the cortical endoplasmic reticulum in saccharomyces cerevisiae. *Journal of Cell Biology*, *150*, 461–474. https://doi.org/10.1083/jcb.150.3.461

Reid, R. J. D., González-Barrera, S., Sunjevaric, I., Alvaro, D., Ciccone, S., Wagner, M., & Rothstein, R. (2011). Selective ploidy ablation, a high-throughput plasmid transfer protocol, identifies new genes affecting topoisomerase I-induced DNA damage. *Genome Research*, *21*, 477–486. https://doi.org/10.1101/gr.109033.110

Rezabakhsh, A., Fathi, F., Bagheri, H. S., Malekinejad, H., Montaseri, A., Rahbarghazi, R., & Garjani, A. (2018). Silibinin protects human endothelial cells from high glucose-induced injury by enhancing autophagic response. *Journal of Cellular Biochemistry*, *119*, 8084–8094. https://doi.org/10.1002/jcb.26735

Ron, D., & Walter, P. (2007). Signal integration in the endoplasmic reticulum unfolded protein response. *Nature Reviews Molecular Cell Biology*, *8*, 519–529. https://doi.org/10.1038/nrm2199

Ryu, T., Spatola, B., Delabaere, L., Bowlin, K., Hopp, H., Kunitake, R., Karpen, G. H., & Chiolo, I. (2015). Heterochromatic breaks move to the nuclear periphery to continue recombinational repair. *Nature Cell Biology*, *17*, 1401–1411. https://doi.org/10.1038/ncb3258

Schuck, S., Gallagher, C. M., & Walter, P. (2014). ER-phagy mediates selective degradation of endoplasmic reticulum independently of the core autophagy machinery. *Journal of Cell Science*, *127*, 4078–4088. https://doi.org/10.1242/jcs.154716

Schuck, S., Prinz, W. A., Thorn, K. S., Voss, C., & Walter, P. (2009). Membrane expansion alleviates endoplasmic reticulum stress independently of the unfolded protein response. *Journal of Cell Biology*, *187*, 525–536. https://doi.org/10.1083/jcb.200907074

Schwarz, D. S., & Blower, M. D. (2016). The endoplasmic reticulum: Structure, function and response to cellular signaling. *Cellular and Molecular Life Sciences*, *73*, 79–94. https://doi.org/10.1007/s00018-015-2052-6

Song, X., Liu, B., Cui, L., Zhou, B., Liu, W., Xu, F., Hayashi, T., Hattori, S., Ushiki-Kaku, Y., Tashiro, S., & Ikejima, T. (2017). Silibinin ameliorates anxiety/depression-like behaviors in amyloid β-treated rats by upregulating BDNF/TrkB pathway and attenuating autophagy in hippocampus. *Physiology & Behavior*, *179*, 487–493. https://doi.org/10.1016/j.physbeh.2017.07.023

Swerdlow, J. L. (2000). *Nature's medicine: Plants that heal*. National Geographic.

Therizols, P., Fairhead, C., Cabal, G. G., Genovesio, A., Olivo-Marin, J. C., Dujon, B., & Fabre, E. (2006). Telomere tethering at the nuclear periphery is essential for efficient DNA double strand break repair in subtelomeric region. *Journal of Cell Biology*, *172*, 189–199. https://doi.org/10.1083/jcb.200505159

Torán-Vilarrubias, A., & Moriel-Carretero, M. (2021). Oxidative agents elicit endoplasmic reticulum morphological changes suggestive of alterations in lipid metabolism. *microPublication Biology*. https://doi.org/10.17912/micropub.biology.000462

Vermeij, W. P., Dollé, M. E. T., Reiling, E., Jaarsma, D., Payan-Gomez, C., Bombardieri, C. R., Wu, H., Roks, A. J. M., Botter, S. M., Van Der Eerden, B. C., Youssef, S. A., Kuiper, R. V., Nagarajah, B., Van Oostrom, C. T., Brandt, R. M. C., Barnhoorn, S., Imholz, S., Pennings, J. L. A., De Bruin, A., & … Hoeijmakers, J. H. J. (2016). Restricted diet delays accelerated ageing and genomic stress in DNA-repair-deficient mice. *Nature*, *537*, 427–431. https://doi.org/10.1038/nature19329

Wang, Q., Liu, W., Zeng, H., Xie, X., Zang, G., Ye, Y., Tashiro, S., Onodera, S., Jiang, S., & Ikejima, T. (2013). p53-mediated autophagy adjustment is involved in the protection of silibinin against murine dermal inflammation and epidermal apoptosis induced by UVB irradiation. *Journal of Asian Natural Products Research*, *15*, 117–129. https://doi.org/10.1080/10286020.2012.739616

Witkin, K. L., Chong, Y., Shao, S., Webster, M. T., Lahiri, S., Walters, A. D., Lee, B., Koh, J. L. Y., Prinz, W. A., Andrews, B. J., & Cohen-Fix, O. (2012). The budding yeast nuclear envelope adjacent to the nucleolus serves as a membrane sink during mitotic delay. *Current Biology*, *22*, R489–R491. https://doi.org/10.1016/j.cub.2012.04.022

Xiao, J., Liu, C. C., Chen, P. L., & Lee, W. H. (2001). RINT-1, a novel Rad50-interacting protein, participates in radiation-induced G2/M checkpoint control. *Journal of Biological Chemistry*, *276*, 6105–6111. https://doi.org/10.1074/jbc.M008893200

Zheng, P., Chen, Q., Tian, X., Qian, N., Chai, P., Liu, B., Hu, J., Blackstone, C., Zhu, D., Teng, J., & Chen, J. (2018). DNA damage triggers tubular endoplasmic reticulum extension to promote apoptosis by facilitating ER-mitochondria signaling. *Cell Research*, *28*, 833–854. https://doi.org/10.1038/s41422-018-0065-z

Abbreviations

DDR	DNA damage response
DSBs	double strand breaks
ER	endoplasmic reticulum
GFP	green fluorescent protein
HR	homologous recombination
RIDD	regulated IRE1α-dependent mRNA decay
UPR	unfolded protein response
WB	western blot
WT	wild type